

Stairway to Success: Zero-Shot Floor-Aware Object-Goal Navigation via LLM-Driven Coarse-to-Fine Exploration

Zeying Gong¹, Rong Li¹, Tianshuai Hu², Ronghe Qiu¹, Lingdong Kong³,
Lingfeng Zhang¹, Yiyi Ding¹, Leying Zhang⁴, Junwei Liang^{1,2*}

¹The Hong Kong University of Science and Technology (Guangzhou)

²The Hong Kong University of Science and Technology

³National University of Singapore

⁴Sun Yat-Sen University

🌐 Project Page: [Link](#) 🐱 Code & Models: [Link](#)

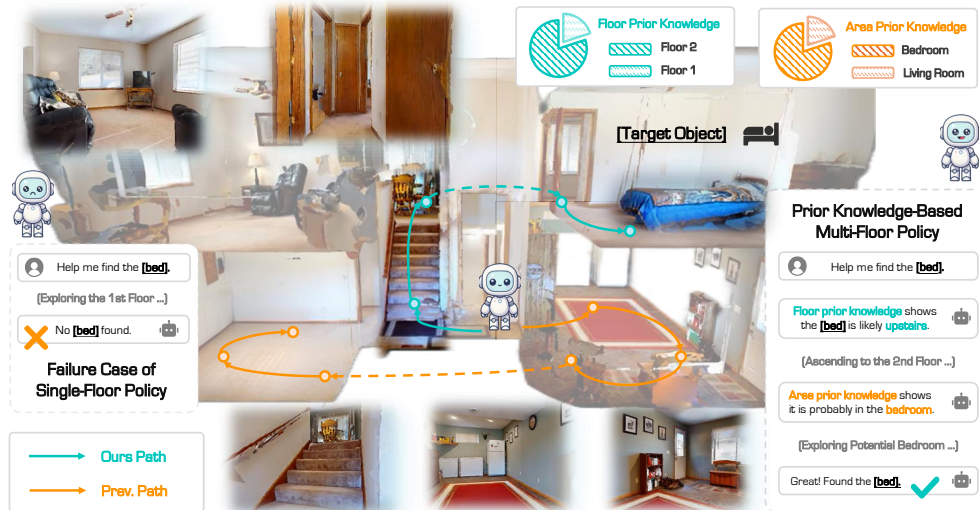


Figure 1: **Motivation of ASCENT.** Our method enables robotic navigation in **unexplored multi-floor environments** under a **zero-shot object-goal setting**, leveraging prior knowledge and coarse-to-fine reasoning to prioritize likely target locations. Unlike previous approaches that struggle with floor-aware planning, our method efficiently handles cross-level transitions and successfully locates objects across floors. This demonstrates a meaningful step forward in zero-shot object-goal navigation field.

Abstract

Object-Goal Navigation (OGN) remains challenging in real-world, multi-floor environments and under open-vocabulary object descriptions. We observe that most episodes in widely used benchmarks such as HM3D and MP3D involve multi-floor buildings, with many requiring explicit floor transitions. However, existing methods are often limited to single-floor settings or predefined object categories. To address these limitations, we tackle two key challenges: (1) efficient cross-level planning and (2) zero-shot object-goal navigation (ZS-OGN), where agents must interpret novel object descriptions without prior exposure. We propose *ASCENT*, a framework that combines a Multi-Floor Spatial Abstraction module for hierarchical semantic mapping and a Coarse-to-Fine Frontier Reasoning module

*Corresponding author: junweiliang@hkust-gz.edu.cn

leveraging Large Language Models (LLMs) for context-aware exploration, without requiring additional training on new object semantics or locomotion data. Our method outperforms state-of-the-art ZS-OGN approaches on HM3D and MP3D benchmarks while enabling efficient multi-floor navigation. We further validate its practicality through real-world deployment on a quadruped robot, achieving successful object exploration across unseen floors.

1 Introduction

Imagine telling a home robot: *‘find the yoga mat’*. It starts searching the bedroom, then the kitchen. When it does not find the object, it pauses and reasons: *“Ah, the yoga mat might be in the gym on the floor below”*. With this insight, it heads toward the stairs to descend and continue its search. This scenario highlights **two key challenges** in Object-Goal Navigation (OGN): First, agents need to **navigate across multiple floors**. Second, they should be able to **interpret open-vocabulary object descriptions** – known as the Zero-Shot Object-Goal Navigation (ZS-OGN) task [47, 43].

To quantify the importance of multi-floor navigation, we analyze the validation sets of two widely used embodied navigation benchmarks: HM3D [38] and MP3D [9]. We find that 65.0% of validation episodes in HM3D and 54.7% in MP3D involve multi-level buildings, with 28.1% and 19.5%, respectively, requiring explicit floor transitions (see Appendix C.1). These findings highlight the critical need for methods capable of effectively addressing multi-floor navigation in the OGN task. However, existing approaches often fail to meet this requirement.

Existing OGN methods can be broadly categorized into *learning-based* and *zero-shot* approaches, yet both fail to address zero-shot multi-floor navigation effectively. Specifically: (1) Learning-based methods [10, 57, 39, 41, 13, 40, 49] are typically trained on specific object categories and environments, which limits their ability to generalize to unseen settings. Our experiments reveal a significant performance drop when these models are applied to new environments (see Appendix B.2). (2) Zero-shot methods [32, 61, 65, 11, 60, 62, 58, 59] mostly overlook the possibility that target objects may reside on different floors or lack the necessary mechanisms for cross-floor navigation. Recent work, such as MFNP [64], treated stairs as irreversible paths, preventing agents from revisiting previously explored floors even when semantic evidence suggests a higher likelihood of finding targets there. This restricts exploration scope and reduces efficiency in multi-floor scenarios.

We address this limitation with our first core contribution: the Multi-Floor Spatial Abstraction module. It builds a unified representation that combines intra-floor and inter-floor relationships, enabling efficient multi-floor path planning and visual navigation.

In addition, navigating in open-world environments introduces another challenge: ZS-OGN requires agents to interpret novel object descriptions using general knowledge. While Large Language Models (LLMs) have shown promise as planners for ZS-OGN, most LLM-based approaches rely on object detectors to convert 3D visual observations into textual descriptions before inputting them to the LLM planner. This process introduces modality discrepancies and leads to information loss. An alternative approach, VLFM [60], uses vision-language models for image-text matching at each step, selecting the frontier point most relevant to the target description. While this avoids explicit object detection, it introduces two key limitations. First, the local matching strategy may yield suboptimal global paths, causing the agent to oscillate between distant frontiers and reducing both Success Rate (SR) and Success Weighted by Path Length (SPL). Second, decisions are made greedily based on current observations, lacking long-term planning and explainability.

Our second core contribution is the Coarse-to-Fine Frontier Reasoning module. It first constructs a value map based on semantic similarity and exploration cost to identify high-priority frontiers, then uses contextual scene descriptions with an LLM for fine-grained reasoning. This improves both navigation efficiency and decision interpretability.

In this work, we propose a zero-shot floor-aware object-goal navigation framework, *ASCENT*, which contains a multi-floor spatial **abstraction** Module to enable making multi-floor navigation decision and a **coarse-to-fine frontier** reasoning module to evaluate prioritized frontiers.

To summarize, the key contributions of this work are:

- We introduce a hierarchical semantic mapping approach that maintains distinct floor-specific representations and inter-floor transitions to enable adaptive multi-floor navigation.
- We design an LLM-based exploration pipeline that integrates semantic similarity and exploration cost into a value map for coarse frontier selection, followed by fine-grained contextual reasoning. This improves navigation efficiency and decision interpretability.
- Our approach achieves state-of-the-art performance for ZS-OGN on HM3D and MP3D benchmarks, improving SR by 7.1% and SPL by 6.8% on HM3D, and 3.4% in SR and 0.1% in SPL on MP3D. We further demonstrate its practicality through sim-to-real deployment on a quadruped robot.

2 Related Work

Object-Goal Navigation. This task involves locating and reaching a target object in unseen environments [6], requiring perception, spatial reasoning, and action planning [15, 19, 25, 17, 26]. As a core capability of embodied AI, it supports downstream tasks such as vision-language navigation [4] and physical interaction [18]. Most prior work employs Reinforcement Learning (RL) [10, 55, 53] or Imitation Learning (IL) [41, 40, 49]. While effective in controlled settings, these methods face key limitations in real-world deployment: RL requires extensive reward annotations [57], IL depends on impractical expert demonstrations [50], and both assume a closed-world setting with fixed object categories [21], failing when encountering novel objects [22].

Zero-Shot Object-Goal Navigation. This task extends OGN by requiring navigation to objects unseen during training [43]. Zhao *et al.* [68] use self-attention to model relationships between seen and unseen classes, but their approach relies on predefined similarity metrics. Zhang *et al.* [67] generate features via adversarial networks, yet their method is limited by static training environments. Cross-task transfer approaches, such as ZESL [2], ZSON [32], and PSL [44], align CLIP embeddings [37] between Image-Goal Navigation (IGN) and OGN. However, these methods inherit spatial biases from IGN that do not match real-world object semantics. A common limitation of them is the need for task-specific training. In contrast, our method operates in a training-free manner.

LLMs for Navigation. Recent advances in Large Language Models (LLMs) enable strong zero-shot generalization in embodied navigation. L3MVN [61] introduces commonsense reasoning, while TriHelper [65] improves long-term planning with dynamic modules. VoroNav [51] combines geometric planning with LLM-based scoring. Recently, GAMap [62] uses affordance attributes for goal localization. SG-Nav [58] proposes a 3D scene graph-based prompting strategy for LLM reasoning. However, current LLM-based methods face two main limitations: (1) they primarily operate on single-floor maps without explicit inter-floor modeling, restricting vertical navigation; and (2) frequent LLM calls to evaluate all frontiers result in high computational cost and limited scalability. In contrast, our Coarse-to-Fine Frontier Reasoning module uses a semantic-value map to filter promising frontiers and invokes the LLM only when necessary to improve efficiency.

3 Methodology

This section firstly introduces the OGN task and presents the overall architecture of *ASCENT*. We then describe our online **Multi-Floor Spatial Abstraction** approach for multi-floor planning, concluding with a **Coarse-to-Fine Frontier Reasoning** strategy that leverages exploration value maps and contextual understanding for zero-shot navigation. An overview of our proposed framework is shown in Fig. 2.

3.1 Problem Formulation

Considering the OGN task for a robot r that starts from an initial configuration $q \in \mathbb{Q}^3$ in an unexplored environment. The robot selects discrete actions $a_t \in \mathcal{A}$ to generate a path τ_r that leads to

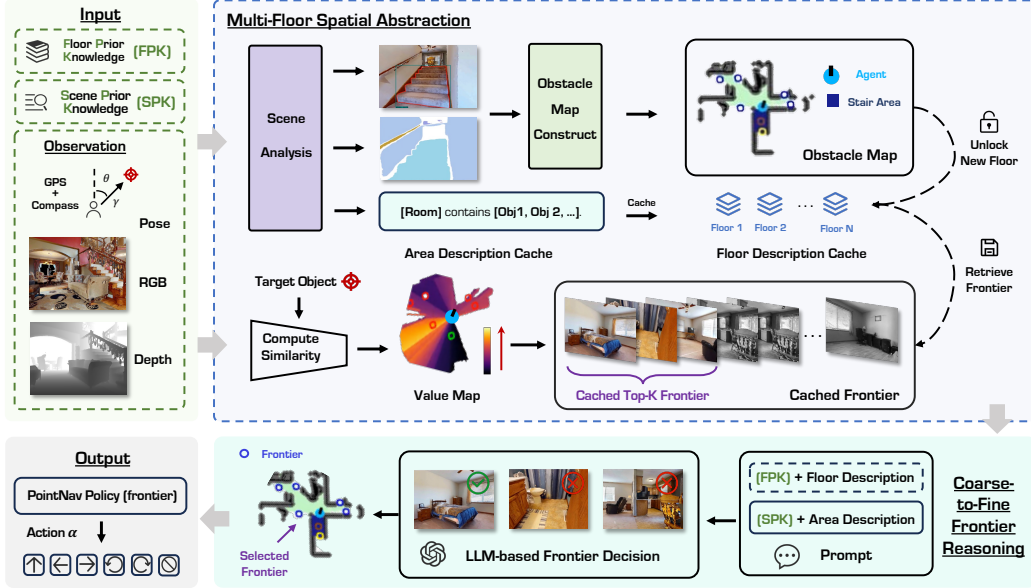


Figure 2: Overview of the *ASCENT* framework. The system takes RGB-D and GPS+Compass inputs (top-left), and uses a pretrained navigation policy (bottom-left) to output actions at each timestep. The Multi-Floor Spatial Abstraction module (top-right) builds single-floor BEV maps and models inter-floor connectivity, enabling cross-level navigation. The Coarse-to-Fine Frontier Reasoning module (bottom-right) selects top-k frontiers based on image-text matching scores and uses an LLM for contextual reasoning across floors, achieving efficient zero-shot, floor-aware object navigation.

the discovery of any instance of a target object category \mathcal{O} . This problem can be formulated as:

$$\tau_r = \arg \min_{\tau \in \mathcal{T}} \left(\underbrace{\lambda_{\text{expl}} c_{\text{expl}}(\tau)}_{\text{exploration cost}} + \underbrace{\lambda_{\text{goal}} c_{\text{goal}}(\tau)}_{\text{exploitation cost}} \right), \quad (1)$$

$$\text{s.t. } \textit{success criteria} : \quad (2)$$

$$\tau(T) \in \{p \in \mathbb{Q}^3 \mid d(p, \mathcal{O}) \leq 1 \text{ m} \wedge a_T = \text{STOP}\}, \quad (3)$$

$$\text{while} : V_r(\tau(t)) \cap V_{\text{obs}} = \emptyset, \forall t \leq T; \quad T \leq T_{\text{max}}. \quad (4)$$

Here, the dual-cost formulation balances *exploration* (i.e., discover unknown areas) and *exploitation* (i.e., efficiently approach targets) via c_{expl} and c_{goal} . $V_r(\tau(t))$ denotes the occupancy volume at time t , and V_{obs} denotes the union of obstacle volumes.

3.2 Framework Overview

Fig. 2 shows the workflow of our proposed framework *ASCENT*, which integrates two core modules: the *Multi-Floor Spatial Abstraction* module for hierarchical semantic mapping and cross-level planning, and the *Coarse-to-Fine Frontier Reasoning* module that uses LLMs for contextual exploration decisions. We describe each module in the following subsections.

3.3 Multi-Floor Spatial Abstraction

To ensure compatibility with standard sim-to-real navigation benchmarks [54, 52], our method operates under 2D localization constraints and avoids reliance on vertical sensor data, which is often noisy or unavailable [7, 33]. Instead, we propose a vision-based, floor-aware modeling strategy that infers inter-floor transitions directly from scene semantics and depth anomalies. This design enables robust multi-floor navigation without requiring explicit height estimation. Due to space limits, kindly refer to Appendix A.4 for detailed motivation and implementations.

3.3.1 BEV Mapping Representations

Our approach draws inspiration from VLFM [60] in terms of using the 2D Bird’s Eye View (BEV) representations for frontier-based navigation. However, we introduce fundamental improvements in three core innovations: (1) an *Exploration Value Map* that combines semantic relevance with spatial cost to improve intra-floor exploration; (2) a *Stair-Aware Obstacle Map*, which dynamically interprets stair-like structures as traversable by the *Stair Detection Module*, ensuring safe inter-floor transitions; and (3) a *Multi-Floor Map Manager* that maintains separate BEV maps per floor and collaborates with the *Cross-Floor Transition Module* to enable robust multi-floor planning.

The core components consist of two complementary 2D BEV mapping representations:

- **Exploration Value Map \mathcal{M}_{val} :** A composite representation fusing (1) a *semantic similarity map*, which measures alignment between each frontier image and the target description; and (2) an *exploration cost map*, which assigns higher values to frontiers surrounded by dense unexplored regions within distance d_{exp} . This design encourages thorough exploration of high-value areas before making high-level decisions. It reduces LLM queries and improves navigation efficiency.
- **Stair-Aware Obstacle Map \mathcal{M}_{obs} :** A binary occupancy grid built from depth data and 2D odometry. Navigable areas and obstacles are updated dynamically based on the robot’s position and field of view. Unlike traditional obstacle maps that ignore or treat stairs as impassable, ours introduces a context-aware interpretation: stair-like structures are semantically labeled as traversable after verification by our detection pipeline. This ensures accurate inter-floor transitions.

3.3.2 Multi-Floor Topology Modeling

To enable semantically-aware multi-floor navigation, we introduce the three key designs (see Appendix C.2 for full implementation):

Stair Detection Module. We detect traversable stairs through a dual-path pipeline combining open-vocabulary detection and RGB-D semantic segmentation. A stair candidate is confirmed only if it satisfies both structural coherence and semantic consistency:

$$S_{\text{valid}} = \left\{ s \in S_{\text{candidate}} \mid D(s) > \epsilon_{\text{stair}} \wedge \frac{\|\text{pixels}_{\text{stair}}(s)\|}{\|\text{pixels}_{\text{region}}(sem)\|} > \epsilon_{\text{sem}} \right\}, \quad (5)$$

where $D(s)$ is the confidence score from the open-vocabulary detector for stair-like structures in region s , $\text{pixels}_{\text{stair}}(s)$ counts pixels labeled as "stair", and $\text{pixels}_{\text{region}}(s)$ is the total pixel count in region s . Thresholds ϵ_{stair} and ϵ_{sem} filter low-confidence candidates and enforce a minimum proportion of stair pixels, respectively (see Appendix C.3). This enables robust stair detection from 2D observations without 3D reconstruction or vertical localization.

Cross-Floor Transition Module. Once a valid stair region is identified, the robot generates a navigation target $\mathcal{F}_{\text{stair}}$ at its midpoint. To ensure stable traversal through potentially unexplored and narrow staircases, we further introduce a dynamic intermediate waypoint located at a fixed distance d_{stair} ahead of the robot’s current pose. Guided by a pretrained point-goal navigation policy, this dual-target strategy enables safe locomotion along the stair structure while reducing the risk of collision or localization drift.

Upon completing the transition, the robot updates its BEV map from the current floor n to either $\mathcal{M}^{(n+1)}$ (ascending) or $\mathcal{M}^{(n-1)}$ (descending), depending on the direction of movement. This mechanism ensures seamless transitions between floor-specific representations and supports consistent multi-floor planning without requiring explicit 3D reconstruction.

Multi-Floor Map Manager. This module maintains dynamic BEV map lists $\mathcal{L}_{\text{obs}} = [\mathcal{M}_{\text{obs}}^{(1)}, \dots, \mathcal{M}_{\text{obs}}^{(N)}]$ and $\mathcal{L}_{\text{val}} = [\mathcal{M}_{\text{val}}^{(1)}, \dots, \mathcal{M}_{\text{val}}^{(N)}]$, where N denotes the total number of explored floors and each entry corresponds to a floor-specific BEV map. In contrast to prior work, MFNP [64], might merge multi-floor data into a single representation, leading to spatial overlap or semantic confusion. Instead, our design preserves per-floor geometry and semantic history to ensure consistent spatial mapping across different floors.



Figure 3: **Illustration of Fine-Grained Context Adaptation.** (a) In multi-floor settings, the agent uses floor-level priors (*e.g.*, object distributions across floors) to decide whether to switch floors. (b) On the current floor, it performs region-level reasoning using room-level object priors and scene descriptions from high-value frontiers.

3.4 Coarse-to-Fine Frontier Reasoning

To enable context-aware exploration in zero-shot, multi-floor environments, we introduce a **Coarse-to-Fine Frontier Reasoning** framework that integrates semantic reasoning with environmental priors. This module operates in two stages: the *Coarse-Grained Frontier Proposal* for computational efficiency, and the *Fine-Grained Context Adaptation* to support robust decision-making.

Before navigation, we incorporate statistical priors on object distributions at both floor and area levels to guide exploration (See Appendix A.2 for details). These priors help align our zero-shot framework with expected object locations and support inter-floor reasoning in the absence of extra information.

3.4.1 Coarse-Grained Frontier Proposal

For each detected frontier, the corresponding RGB image at that timestep is processed to generate a structured scene description using a scene classification model and an image tagging model. These descriptions capture both room types (*e.g.*, “living room”) and associated objects (*e.g.*, “sofa”), forming a rich contextual basis for LLM reasoning.

To further improve efficiency (reduce redundancy), we apply visual similarity filtering using Structural Similarity Index Measure (SSIM) [48], removing frontiers whose representative images exceed a threshold ϵ_{ssim} on structural overlap. This ensures spatial diversity among candidates, avoiding repetitive evaluations of visually similar regions. Descriptions are cached for use in the later timesteps of the episode, minimizing repeated computation. Detailed descriptions are placed in Appendix A.5.

3.4.2 Fine-Grained Context Adaptation

The agent activates the aforementioned procedures only when multiple distinct frontiers are present and no new ones are detected within a radius d_{fine} , indicating sufficient local exploration. As shown in Fig. 3, this stage involves the following two aspects:

(1) *Inter-Floor Floor Decision.* Given multiple available floors, the agent decides whether to stay or transition using learned floor-level priors over object distributions and exploration status. An LLM evaluates this context and selects a target floor if switching is beneficial, while a policy prevents frequent transitions by requiring a minimum dwell time ϵ_{mf} or full floor coverage.

(2) *Intra-Floor Frontier Decision.* Within the selected floor, the agent analyzes semantic descriptions of each frontier (*e.g.*, room type, object presence) together with the task instruction (*e.g.*, “find the cabinet”) to prioritize the most relevant location via LLM-based reasoning.

This hierarchical design balances computational efficiency and contextual relevance, enabling effective zero-shot navigation without explicit training on object-specific categories.

Table 1: **Quantitative comparisons of OGN task** on the *HM3D* [38] and *MP3D* [9] datasets. The table contrasts supervised and zero-shot methods across the “*Success Rate*” (SR) and “*Success Weighted by Path Length*” (SPL) metrics, respectively, highlighting the state-of-the-art performance of our approach in open-vocabulary and multi-floor navigation scenarios.

	Method	Venue	Instruction Interpolator		HM3D [38]		MP3D [9]	
			Vision	Language	SR ↑	SPL ↑	SR ↑	SPL ↑
Setting: Close-Set								
Single-Floor	SemExp [10]	NeurIPS’20	-	-	37.9	18.8	36.0	14.4
	Aux [57]	ICCV’21	-	-	-	-	30.3	10.8
	PONI [39]	CVPR’22	-	-	-	-	31.8	12.1
	Habitat-Web [41]	CVPR’22	-	-	41.5	16.0	35.4	10.2
	RIM [13]	IROS’23	-	-	57.8	27.2	50.3	17.0
Multi-Floor	PIRLNav [40]	CVPR’23	-	-	64.1	27.1	-	-
	XGX [49]	ICRA’24	-	-	72.9	35.7	-	-
Setting: Open-Set								
Single-Floor	ZSON [32]	NeurIPS’22	CLIP [37]	-	25.5	12.6	15.3	4.8
	L3MVN [61]	IROS’23	-	⊗ GPT-2 [30]	50.4	23.1	34.9	14.5
	SemUtil [12]	RSS’23	-	BERT [14]	54.0	24.9	-	-
	CoW [16]	CVPR’23	CLIP [37]	-	32.0	18.1	-	-
	ESC [69]	ICML’23	-	⊗ GPT-3.5 [34]	39.2	22.3	28.7	14.2
	PSL [44]	ECCV’24	CLIP [37]	-	42.4	19.2	-	-
	VoroNav [51]	ICML’24	BLIP [24]	⊗ GPT-3.5 [34]	42.0	26.0	-	-
	PixNav [8]	ICRA’24	LLaMA-Adapter [66]	⊗ GPT-4 [1]	37.9	20.5	-	-
	Trihelper [65]	IROS’24	⊗ Qwen-VLChat-Int4 [5]	⊗ GPT-2 [30]	56.5	25.3	-	-
	VLFM [60]	ICRA’24	BLIP-2 [23]	-	52.5	30.4	36.4	17.5
	GAMap [62]	NeurIPS’24	CLIP [37]	⊗ GPT-4V [1]	53.1	26.0	-	-
	SG-Nav [58]	NeurIPS’24	LLaVA-1.6-7B [28]	⊗ GPT-4 [1]	54.0	24.9	40.2	16.0
	InstructNav [31]	CoRL’24	-	⊗ GPT-4V [1]	58.0	20.9	-	-
	UniGoal [59]	CVPR’25	LLaVA-1.6-7B [28]	LLaMA-2-7B [45]	54.0	24.9	41.0	16.4
	Multi-Floor	MFNP [64]	ICRA’25	⊗ Qwen-VLChat-Int4 [5]	⊗ Qwen2-7B [30]	58.3	26.7	41.1
ASCENT		Ours	BLIP-2 [5]	⊗ Qwen2.5-7B [56]	65.4	33.5	44.5	15.5

4 Experiments

4.1 Experimental Settings

Data. We evaluate our method on two real-world, multi-floor indoor datasets using the Habitat simulator [42]. **HM3D** [38] contains 2,000 validation episodes across 20 scenes with 6 object categories, covering complex residential and commercial environments. **MP3D** [9] includes 2,195 validation episodes across 11 scenes and spans 21 object categories (with 6 shared with HM3D), offering a broader testbed for performance and generalization.

Implementation Details. Our experiments are conducted on Habitat 3.0 [36], building upon the VLFM architecture [60]. We use D-FINE [35] for COCO-class objects [27] and Grounding-DINO [29] for open-vocabulary detection. Object contours are segmented by Mobile-SAM [63], and stair detection integrates a fine-tuned RedNet [20] with RGB-D inputs. BLIP-2 [24] computes semantic similarity, and Qwen2.5-7B-Instruct [56] performs LLM-based reasoning. All experiments were run on a single compute node with two NVIDIA RTX 3090 GPUs.

Evaluation Metrics. We adopt two standard metrics from [3]: Success Rate (SR) and Success weighted by Path Length (SPL). See Appendix A.3 for more details.

4.2 Comparisons to State-of-the-Arts

Our method establishes a new state-of-the-art in zero-shot object-goal navigation on both HM3D and MP3D. On HM3D, we achieve 65.4% SR and 33.5% SPL, improving upon the previous zero-shot multi-floor SOTA MFNP [64] by +7.1% in SR and +6.8% in SPL. On MP3D, we reach 44.5% SR and 15.5% SPL, outperforming MFNP by +3.4% in SR with nearly identical SPL. Compared to VLFM [60], our approach underperforms slightly in path efficiency (−2.0% SPL), but achieves significantly higher success rate (+8.1% SR). This is because VLFM is limited to single-floor

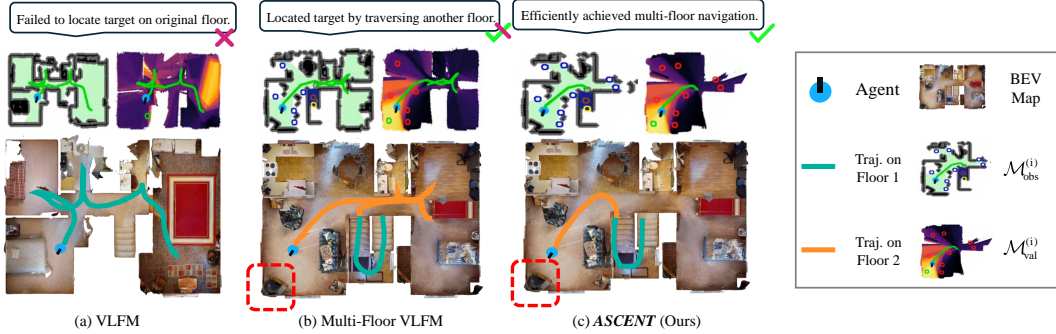


Figure 4: **Comparisons of methods in multi-floor environments.** (a) VLFM [60] fails to navigate to another floor, resulting in a low success rate (SR). (b) Adding the Multi-Floor Spatial Abstraction module to VLFM [60] allows reaching different floors but often leads to unnecessarily long paths. (c) Our method efficiently navigates across floors and selects the nearly optimal path to the target.

Table 2: Effect of key components of *ASCENT* on *HM3D* [38] dataset.

Method	SR \uparrow	SPL \uparrow	DTG \downarrow
w/o ECM	56.3	27.7	4.335
w/o MFTM	56.7	28.6	3.964
w/o CFFR	57.7	28.5	3.899
w/o PK	62.1	30.1	3.434
<i>ASCENT</i> (Ours)	65.4	33.5	2.934

Table 3: Ablation study of large models on zero-shot multi-floor settings. The results marked with † were obtained via direct communication with the authors.

Method	Instruction Interpolator		HM3D		MP3D	
	Vision	Language	SR \uparrow	SPL \uparrow	SR \uparrow	SPL \uparrow
MFNP	Qwen-VLChat-Int4	Qwen2-7B	58.3	26.7	41.1	15.4
MFNP†	BLIP-2	Qwen2.5-7B	55.8	24.9	38.5	12.4
Ours	BLIP-2	Qwen2.5-7B	65.4	33.5	44.5	15.5

navigation, while our framework enables cross-level transitions, where floor switching improves overall success at the cost of longer paths.

Although our performance lags behind leading supervised methods such as XGX [49] and RIM [13], our framework operates entirely without task-specific training data, which makes it well-suited for sim-to-real deployment. As shown in Appendix B.2, these supervised approaches exhibit significant performance drops when transferred to unseen environments or novel object categories, whereas our method remains robust across domains. This confirms that *ASCENT* has achieved strong performance without labeled data and demonstrated superior generalization capabilities, setting a new standard in zero-shot, floor-aware navigation.

4.3 Qualitative Analysis

In Fig. 4, we illustrate the navigation process of *ASCENT*. The top row shows the trajectory of our primary baseline method, VLFM. In this scenario, the target object is located on the second floor, while the agent starts on the first floor. Traditional methods like VLFM, which lack multi-floor navigation capabilities, terminate after traversing the first floor. The middle row demonstrates that when VLFM is enhanced with multi-floor capabilities through the MFMT module, it successfully navigates to the second floor and reaches the target object. However, it nearly exhaustively explores the second floor, resulting in lower path efficiency. In contrast, our method not only supports multi-floor navigation but also selects a nearly optimal path to the target object upon reaching the second floor. This leads to higher SR and better SPL.

4.4 Ablation Study

Effect of Both Intra-Floor and Inter-Floor Strategies. As shown in Tab. 4, our method achieves consistent improvements over the baseline approach VLFM and the state-of-the-art zero-shot method MFNP, across all scenarios of single-floor and multi-floor settings. In single-floor settings, *ASCENT* attains 76.1% SR (6.3% absolute gain vs VLFM) with 22% closer to targets than VLFM, demonstrating enhanced intra-floor exploration through our Coarse-to-Fine Frontier Reasoning. The multi-floor results reveal even more significant advantages: *ASCENT* outperforms MFNP by 7.1% SR and 7.4%

Table 4: Navigation performance comparison on the *HM3D* [38] dataset. in single-floor, multi-floor, and all scenarios. The results marked with † were obtained via direct communication with the authors.

Method	Single-Floor Scenarios			Multi-Floor Scenarios			All Scenarios		
	SR↑	SPL↑	DTG↓	SR↑	SPL↑	DTG↓	SR↑	SPL↑	DTG↓
VLFM	69.8	38.2	2.049	43.9	25.3	5.303	52.8	30.5	4.149
MFNP†	69.4	33.5	2.518	52.6	23.1	4.127	58.3	26.7	3.568
ASCENT (Ours)	76.1	39.0	1.591	59.7	30.5	3.646	65.4	33.5	2.934

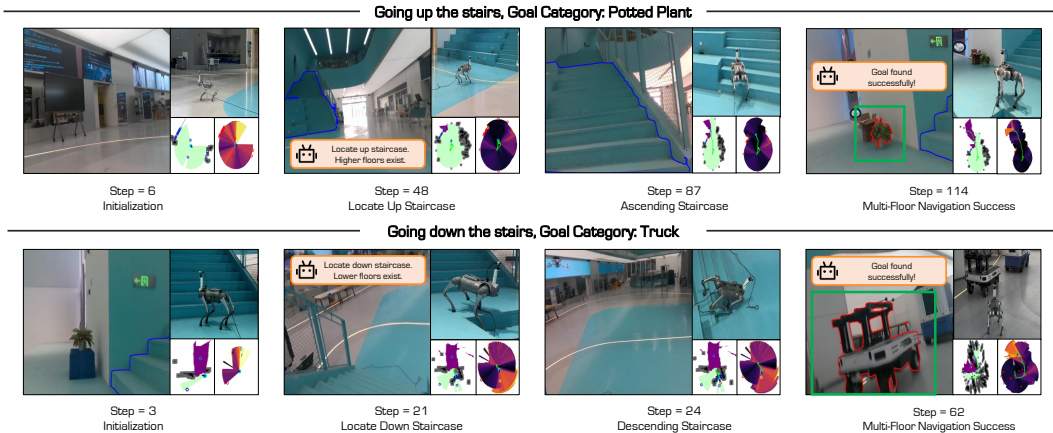


Figure 5: Sim-to-Real demonstration of *ASCENT* with a quadruped robot in real-world environments.

SPL while reducing navigation distance by 11.6%, validating the effectiveness of our framework in resolving inter-floor transitions.

Effect of Architecture Design. Tab. 2 presents the ablation study of our framework components on the HM3D dataset. In addition to standard metrics, we report Distance to the Goal (DTG), which measures the geodesic distance from the final position to the closest target, offering finer insights into localization accuracy. Removing the Multi-Floor Topology Modeling (MFTM) module leads to the most significant performance drop: -8.7% SR and -4.9% SPL, highlighting its critical role in multi-floor navigation. Disabling the Coarse-to-Fine Frontier Reasoning (CFFR) module results in a -7.7% SR and -5.0% SPL decline, underscoring its importance in guiding efficient exploration.

Without the Exploration Cost Map (ECM), the agent suffers -9.1% SR and -5.8% SPL degradation, indicating its necessity in avoiding costly paths. When prior knowledge (PK) is removed, the performance decreases only moderately (-3.3% SR and -3.4% SPL). This suggests that while LLMs inherently encode sufficient world knowledge and spatial reasoning capabilities for zero-shot navigation, the integration of statistical priors provides a structured reference that further aligns the agent’s behavior with environmental regularities.

Effect of Large Models. We conduct an ablation study on the large model in Tab. 3, by replacing the original Instruction Interpolator components in MFNP (the previous SOTA method) with the configuration of our model: substituting Qwen-VLChat-Int4 with BLIP-2 for vision and Qwen2-7B with Qwen2.5-7B for language processing. Surprisingly, this modification (MFNP*) leads to performance degradation, with SR dropping from 58.3% to 55.8% and SPL decreasing from 26.7% to 24.9%. This ablation highlights that our improvements stem from novel algorithm design rather than simply employing more powerful foundation models.

4.5 Sim-to-Real Deployment

We conduct real-world experiments on the Unitree quadruped robot *Go2* to demonstrate the practical effectiveness of *ASCENT*. The robot uses a RealSense D435i Camera for RGB-D perception and its Inertial Measurement Unit (IMU) for pose estimation. Fig. 5 shows successful multi-floor navigation, including stair ascent and descent, validating the generalization of our method in real-world settings.

The core planning strategy runs on an external laptop with an RTX 2060 GPU, connected to the robot via Ethernet for real-time execution through the SDK. LLM-based reasoning and high-level decision-making are offloaded to a remote server with two RTX 3090 GPUs, communicating with the laptop over a wireless network. Similar to our simulation setup, the agent’s low-level actions are generated by a pretrained PointNav Policy of VLFM [60], ensuring stable locomotion while allowing our framework to focus on high-level semantic reasoning.

5 Conclusion

We presented *ASCENT*, a floor-aware ZS-OGN framework that addresses the limitations of existing methods in multi-floor and open-vocabulary settings. Our approach combines a hierarchical multi-floor spatial abstraction with a coarse-to-fine frontier reasoning strategy, enabling efficient cross-floor planning and context-aware exploration without requiring task-specific training or finetuning. Experimental results on HM3D and MP3D benchmarks show that *ASCENT* outperforms state-of-the-art zero-shot methods. We further validated its real-world applicability through sim-to-real deployment on a Unitree quadruped robot, demonstrating successful multi-floor navigation in unseen real-world environments. This work contributes to the field by offering a training-free, general-purpose solution that bridges the gap between semantic understanding and multi-floor navigation.

Appendix

A Additional Implementation Details	11
A.1 Hyperparameters	11
A.2 Motivation of Prior Knowledge	11
A.3 More Details of Object-Goal Task	11
A.4 Vertical Localization Constraints	11
A.5 Implementation Details of Coarse-Grained Frontier Proposal	12
B Additional Ablation Experiments	12
B.1 Effect of Object Detectors.	13
B.2 Comparisons of Generalization Performance.	13
C Details of Multi-Floor Navigation	14
C.1 Motivation of Multi-Floor Navigation	14
C.2 Implementation Details of Multi-Floor Topology Modeling	15
C.3 Stair Detection Visualization for Multi-Floor Navigation	16
C.4 Cases Analysis for Stair Ascending	16
C.5 Cases Analysis for Stair Descending	17
C.6 Cases Analysis for Stairwells	18
C.7 Cases Analysis for Floor Revisiting	18
D Discussions & Limitations	19
E Detailed Prompt Design	21

A Additional Implementation Details

In this section, we elaborate on additional experimental settings and implementation details to facilitate the reproduction of the approach proposed in this work.

A.1 Hyperparameters

Tab. 5 outlines the key hyperparameters used in the *ASCENT* framework. Note that we disable random sampling of LLM to guarantee output stability and consistency. The detection thresholds for object detection models are referenced from the VLFM [60], which serves as our baseline for comparison.

A.2 Motivation of Prior Knowledge

Before navigation, we extract statistical priors from the training sets of corresponding large-scale datasets, including *floor-level* and *area-level* object distributions. These priors serve two key purposes: First, they reflect dataset-specific patterns that learning-based methods may implicitly encode, which provides a structured reference for our zero-shot framework to align with expected object locations. Second, in the absence of global map knowledge, they offer valuable guidance for inter-floor reasoning, helping the agent prioritize unexplored floors or areas where target objects are more likely to appear based on environmental context.

Incorporating prior knowledge into our system is designed to enhance performance, although it is not essential for the core functionality. The Floor Prior Knowledge is derived from the training data of the HM3D and MP3D datasets, which are tailored to match the characteristics of their respective test datasets. This approach improves the spatial understanding necessary for multi-floor navigation tasks. The Scene Prior Knowledge is gleaned from the statistical properties of the HM3D dataset, which enriches the LLM’s comprehension of common scene elements and their typical configurations.

As discussed in Tab. 2, we have already explored the influence of this prior knowledge. The LLM possesses inherent capabilities that enable it to adapt and deliver sensible outputs even in the absence of prior knowledge. Nevertheless, when augmented with the statistical insights gleaned from the datasets, the LLM operates more efficiently and with enhanced accuracy, thereby offering a marginal improvement in performance.

A.3 More Details of Object-Goal Task

Our navigation framework operates under a discrete action space \mathcal{A} , defined as follows:

- MOVE-FORWARD: Move forward by 0.25 m.
- TURN-LEFT: Rotate left by 30°.
- TURN-RIGHT: Rotate right by 30°.
- LOOK-UP: Tilt camera upward by 30°.
- LOOK-DOWN: Tilt camera downward by 30°.
- STOP: Terminate the episode.

This action set is consistent with standard embodied AI benchmarks such as the Habitat [42] and Matterport3D environments [9], ensuring fair comparison and sim-to-real compatibility.

Each episode has a maximum time limit of $T_{\max} = 500$ steps. If the agent fails to locate the target object within this limit, the episode terminates without success. This constraint reflects real-world deployment scenarios where task efficiency and response time are critical. The episode is considered successful only when the agent executes the STOP action within 1 meter of any instance of the target object category.

A.4 Vertical Localization Constraints

In real-world settings, precise vertical localization remains challenging due to sensor limitations and environmental factors. Widely used benchmarks such as the Habitat Navigation Challenge [54, 52]

Table 5: Hyperparameters of *ASCENT*.

Parameter	Value
LLM Temperature	0
Grounding-DINO Detection Threshold $\epsilon_{\text{non-coco}}$	0.4
Grounding-DINO Detection for Stair Threshold ϵ_{stair}	0.6
D-FINE Detection Threshold ϵ_{coco}	0.8
YOLOv7 Detection Threshold	0.8
Semantic Pixel Ratio Threshold ϵ_{sem}	0.33
SSIM Score Threshold ϵ_{SSIM}	0.85
Top k Frontier Candidates	3
Exploration Distance d_{exp} for ECM	3.0
Dynamic Waypoint Distance on Stair d_{stair}	0.8
Multi-Floor Decision Dwell Time $\epsilon_{m.f}$	60

constrain agents to GPS+Compass sensors that provide only 2D horizontal localization, ensuring fair comparison across methods and reflecting practical sim-to-real constraints.

IMU-derived height estimates are prone to drift and lack precision during dynamic movements like stair climbing [7]. Visual SLAM also struggles in texture-poor environments such as staircases, where feature extraction becomes unreliable [33]. Even if vertical coordinates were available, determining floor levels would still require knowledge of building-specific floor heights. However, prior information is typically unknown in unseen environments. Small sensor errors could lead to incorrect floor classification and planning failures.

Instead of relying on noisy or unavailable vertical data, we propose a vision-based, floor-aware modeling strategy that infers inter-floor transitions directly from scene semantics and depth anomalies. This approach offers a more robust and realistic solution for multi-floor navigation under RGB-D and 2D odometry constraints.

A.5 Implementation Details of Coarse-Grained Frontier Proposal

Frontiers are defined as the boundary midpoints between explored and unexplored regions. For each detected frontier, the corresponding RGB image at that timestep is processed to generate a structured scene description using a scene classification model and an image tagging model. These descriptions capture both room types (*e.g.*, “living room”) and associated objects (*e.g.*, “sofa”, “TV”), forming a rich contextual basis for LLM reasoning.

To further improve efficiency and reduce redundancy, we apply a visual similarity filter to remove the frontiers whose representative images stay below a threshold θ on structural overlap. This design prioritizes frontiers based on scene semantics and spatial diversity:

$$\mathcal{F}_{\text{coarse}} = \{f \in \mathcal{F}_{\text{boundary}} \mid \text{SSIM}(f, \mathcal{F}_{\text{cache}}) < \tau_{\text{ssim}}\}, \quad (6)$$

where $\mathcal{F}_{\text{boundary}}$ denotes frontier boundary points between explored and unexplored regions, and $\mathcal{F}_{\text{cache}}$ stores previously evaluated frontiers. The Structural Similarity Index Measure (SSIM) [48] quantifies perceptual similarity between image pairs by comparing luminance, contrast, and structure:

$$\text{SSIM}(x, y) = \frac{(2\mu_x\mu_y + c_1)(2\sigma_{xy} + c_2)}{(\mu_x^2 + \mu_y^2 + c_1)(\sigma_x^2 + \sigma_y^2 + c_2)}, \quad (7)$$

where μ , σ , and σ_{xy} denote local means, standard deviations, and cross-covariance of image intensities, respectively; c_1 and c_2 are small constants to stabilize division. We use this metric to filter out visually redundant frontiers, ensuring spatial diversity in the candidate set.

B Additional Ablation Experiments

In this section, we delve into more ablation experiments to provide a comprehensive understanding of how different factors, such as the choice of large models and object detectors, impact the overall

Table 6: Comparative results of different object detectors.

Method	Object Detector	HM3D		MP3D	
		SR \uparrow	SPL \uparrow	SR \uparrow	SPL \uparrow
VLFM	GroundingDINO + YOLOv7	52.5	30.4	36.4	17.5
	GroundingDINO + D-FINE	54.1	33.0	37.5	17.8
	Ideal	62.4	40.0	55.3	29.6
<i>ASCENT</i> (Ours)	GroundingDINO + YOLOv7	60.9	29.6	42.4	13.8
	GroundingDINO + D-FINE	65.4	33.5	44.5	15.5
	Ideal	70.3	41.0	58.6	30.3

Table 7: Generalization performance. Closed-set learning methods show poor transferability, while our zero-shot method achieves strong cross-dataset generalization.

Method	Training Scenes	Zero-Shot	Open-Set	HM3D		MP3D	
				SR \uparrow	SPL \uparrow	SR \uparrow	SPL \uparrow
RIM [13]	MP3D	✗	✗	57.8	27.2	50.3	17.0
PIRLNav [40]	HM3D	✗	✗	64.1	27.1	8.6	2.7
XGX [49]	HM3D	✗	✗	72.9	35.7	13.6	5.1
<i>ASCENT</i> (Ours)	–	✓	✓	65.4	33.5	44.5	15.5

performance of our framework. Specifically, we first investigate the influence of employing different large models in our architecture and then explore the role of object detectors in enhancing navigation performance. The results of these ablation studies not only highlight the strengths of our method but also offer insights into potential areas for further improvement.

B.1 Effect of Object Detectors.

We also conduct an ablation study on the object detector in Tab. 6, revealing three key insights: (1) When using YOLOv7 [46] (equivalent to VLFM’s detector), our framework still outperforms VLFM by 8.4% SR, validating our architecture’s superiority beyond sensing capabilities; (2) Adopting the state-of-the-art object detector D-FINE [35] further improves navigation performance (+4.5% SR), confirming our framework’s ability to leverage detection advances. (3) We employ a perfect object detector, *i.e.*, ground truth semantic segmentation sensor, which results in an additional 4.9% improvement in SR and a 7.6% increase in SPL.

This finding is consistent with the target-triggered nature of our object navigation approach, where reliable object-goal detection is crucial for triggering the stage transition from exploration to exploitation. The significant performance boost under ideal detection conditions not only highlights the potential of our method but also provides an indication of its theoretical upper bound.

B.2 Comparisons of Generalization Performance.

To evaluate the generalization ability of closed-set methods and our method, we compare the most advanced learning-based methods (RIM[13], PIRLNav [40], and XGX [49]) with our zero-shot approach on both HM3D and MP3D datasets. As shown in Tab. 7, the learning-based methods exhibit strong performance on the training dataset (HM3D) but suffer significant drops in SR and SPL when transferred to MP3D, highlighting their struggle to generalize to unseen environments. In contrast, our zero-shot method maintains robust performance across both datasets, achieving the best SR on MP3D and demonstrating superior generalization ability.

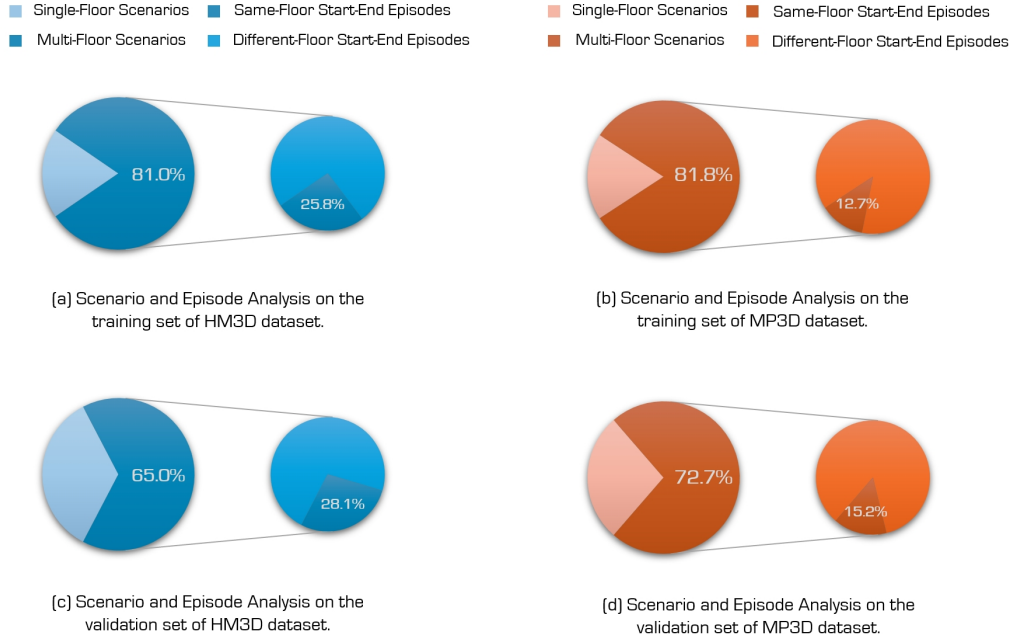


Figure 6: **Multi-Floor Scene and Episode Analysis.** We observe that over half of the scenarios involve multiple floors, with approximately one-fifth of episodes requiring cross-floor capabilities for the agent, consistent across the training and validation sets of two public benchmarks.

C Details of Multi-Floor Navigation

The Multi-Floor Spatial Abstraction module is a key innovation of our work, enabling floor awareness for the agent and serving as a plug-and-play module for navigation tasks. This section details its working principle and navigation impact through both textual description and visual analysis.

C.1 Motivation of Multi-Floor Navigation

As mentioned in Sec. section 1, our motivation for multi-floor navigation stems from both simulated datasets and real-world observations. In the two photorealistic public datasets we utilized, multi-floor scenarios constitute a significant portion, as shown in Fig. 6: approximately 65.0% of validation scenarios in HM3D and 54.7% of validation scenarios in MP3D. In reality, buildings are often designed with multiple floors to maximize land resource utilization. This indicates that multi-floor navigation is an important and promising direction, both in simulation and real-world applications. Furthermore, in these multi-floor scenarios, the proportion of episodes where the target is located on a different floor from the starting point is about 19.5% in HM3D and 28.1% in MP3D. Notably, these divisions are calculated based on height, and in real environments, transitions between floors involve stairs or stairwells. These transitional areas require the system not only to understand the layout of cross-floor areas but also to effectively plan and navigate between different floors, which is a more complex capability for navigation.

Currently, most navigation systems overlook the cross-floor capabilities required for such tasks, leading to failures in these episodes and creating bottlenecks in success rates. As shown in Fig. 7, previous LLM-Planners, with the exception of MFNP, often lack multi-floor navigation capabilities. They either fail to move between floors or do not recognize when a floor change has occurred, resulting in semantic map confusion or overlap. While MFNP can detect upstairs transitions through image recognition and perform cross-floor detection, it struggles with downstairs transitions (since downstairs stairs are not directly visible from the default horizontal perspective). This limits its cross-floor capabilities. Additionally, MFNP treats stair entrances as obstacles to prevent floor transition failures, which inadvertently prevents re-visiting floors. Although learning-based methods can handle multi-floor navigation, they lack interpretability in cross-floor reasoning and planning, and

	Open-Set 	Training-Free 	Ascend Stairs 	Descend Stairs 	Cross-Floor Reasoning 	Floor Revisiting 
Learning-based Methods	✗	✗	✓	✓	✗	✓
Prior LLM-Planners	✓	✓	✗	✗	✗	✗
MFNP	✓	✓	✓	✗	✓	✗
ASCENT (Ours)	✓	✓	✓	✓	✓	✓

Figure 7: Capability comparisons of navigation methods.

they fail to generalize to open-vocabulary detection tasks. This has inspired us to explore adaptive multi-floor navigation algorithms that address these limitations.

C.2 Implementation Details of Multi-Floor Topology Modeling

Stair Detection Module. Inter-floor transitions are resolved through a dual-path detection pipeline that adapts to ascending and descending scenarios. For upward stair detection, we first identify candidate regions using an open-vocabulary detector, which localizes stair-like structures in the agent’s frontal RGB view. These candidates undergo cross-modal validation: a concurrent semantic segmentation branch based on RGB-D evaluates pixel-wise "stair" class coverage. A transition is confirmed only when a significant portion δ of the detected region exhibits coherent structure and semantic labels. This ensures robust identification of traversable stairs.

Downward stair recognition poses additional challenges. Since stairs are not directly visible from a horizontal viewpoint ($\phi = 0^\circ$), many existing methods fail to detect them accurately. As a result, they often produce incorrect floor-level identification and cause semantic map mixing. To address this issue, we employ depth anomaly analysis. Projecting depth measurements onto a ground plane reveals regions where points fall below the estimated floor level and exhibit abrupt depth discontinuities. These anomalies trigger active sensing: the agent tilts its camera to $\phi = -30^\circ$ and approaches for direct observation. The same cross-modal validation used for ascending stairs confirms descending transitions. This leads to the retrieval or creation of lower-floor maps in \mathcal{L}_{obs} , ensuring bidirectional topological consistency.

Cross-Floor Transition Module. Once a stair transition is confirmed, the agent initiates floor-level movement using the midpoint of the largest stair region, which is registered as a stair frontier $\mathcal{F}_{\text{stair}}$, as a navigation waypoint. The navigation strategy for both ascending and descending stairs follows a similar principle: the agent evaluates semantic coverage within the detected stair region to determine whether the structure is sufficiently visible and traversable. If the coverage meets a threshold indicating reliable visibility, the agent adjusts its pitch angle accordingly (LOOK-UP for ascending, LOOK-DOWN for descending) and proceeds with a sequence of forward actions while updating its position in the corresponding floor map.

To ensure safe traversal after reaching the stair frontier, we introduce a dynamic waypoint positioned at a distance ahead of the robot. This waypoint is continuously updated based on the robot’s pose to guide the agent through narrow or occluded regions where depth information becomes unreliable. Once the entire robot exits the semantic stair region, it resets its pitch angle and initializes a new floor map if necessary.

Multi-Floor Map Manager. To ensure topological consistency across multiple floors and avoid semantic confusion, our system maintains separate BEV maps for each explored floor:

$$\mathcal{L}_{\text{obs}} = [\mathcal{M}_{\text{obs}}^{(1)}, \dots, \mathcal{M}_{\text{obs}}^{(N)}], \quad \mathcal{L}_{\text{val}} = [\mathcal{M}_{\text{val}}^{(1)}, \dots, \mathcal{M}_{\text{val}}^{(N)}], \quad (8)$$

where N is the number of explored floors, $\mathcal{M}_{\text{obs}}^{(n)}$ represents the obstacle map for floor n , and $\mathcal{M}_{\text{val}}^{(n)}$ encodes the exploration value map that fuses semantic relevance and spatial cost.

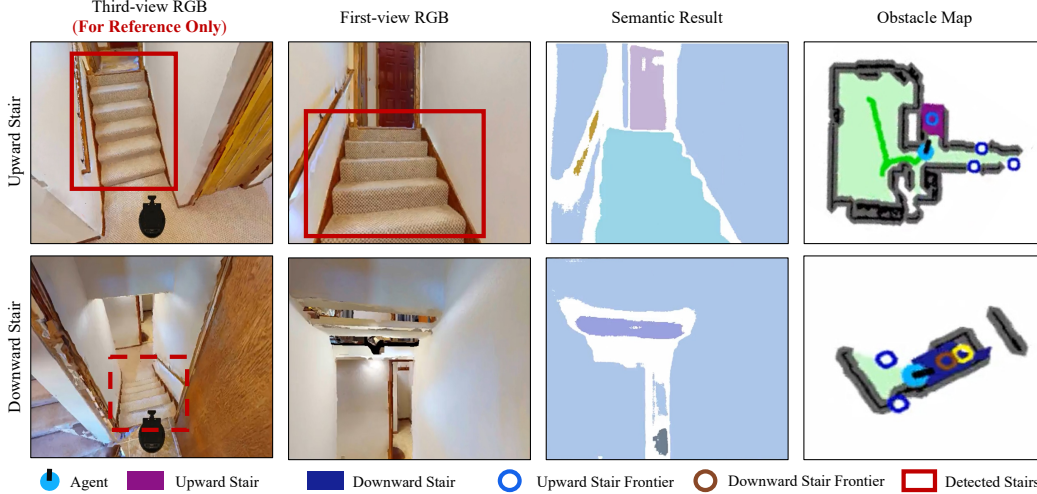


Figure 8: **Stair Detection and Inference.** **Top row:** Direct detection of ascending stairs through visual perception modules. **Bottom row:** Indirect inference of descending stairs via depth analysis and downward verification.

These maps are maintained in a shared polar coordinate system (ρ, θ, z) , enabling seamless cross-floor planning while adhering to RGB-D and 2D odometry constraints. Floor-specific representations are dynamically updated during navigation and initialized only upon verified inter-floor transitions, reducing memory overhead and avoiding spatial overlap.

Moreover, the BEV maps for unexplored floors are initialized only upon verified stair transitions, with dedicated handling for ascending ($\mathcal{M}^{(n+1)}$) or descending ($\mathcal{M}^{(n-1)}$) cases. This strategy avoids redundant mapping and significantly reduces memory overhead by eliminating the need for full 3D reconstruction. All maps are aligned within a global polar coordinate system (ρ, θ, z) , therefore, this unified workflow ensures seamless 3D environment awareness while strictly adhering to RGB-D and 2D odometry constraints.

C.3 Stair Detection Visualization for Multi-Floor Navigation

As illustrated in Fig. 8, our framework enables robust multi-floor navigation through two complementary perception strategies: direct detection of ascending stairs and active inference of descending stairs. For upward transitions, we leverage multi-modal visual perception (object detection and semantic segmentation) to identify stairs within the agent’s immediate field of view. In contrast, downward transitions pose a unique challenge due to their initial occlusion; our system first hypothesizes their presence by depth inversion analysis, then actively verifies them by executing a LOOK-DOWN action to tilt the camera downward, ensuring geometric consistency before committing to the transition. This asymmetric approach—combining direct recognition with depth-guided inference—ensures reliable stair awareness across diverse real-world environments.

C.4 Cases Analysis for Stair Ascending

When the target is located on a higher floor, the agent must navigate upstairs. As shown in Fig. 9, the process for upstairs navigation is as follows:

Initially, the agent operates under the assumption of a single floor, using BEV map lists $\mathcal{L}_{obs} = [\mathcal{M}_{obs}^{(1)}]$ and $\mathcal{L}_{val} = [\mathcal{M}_{val}^{(1)}]$, performing intra-floor navigation until detecting an upstairs region through both staircase detection and semantic segmentation. Upon detection, it initializes maps for the higher floor ($\mathcal{M}_{obs}^{(2)}, \mathcal{M}_{val}^{(2)}$).

The agent initiates upstairs transition when either: (1) the current floor exploration completes while higher unexplored floors remain, as shown in the example of the top row in Fig. 9; or (2) the step

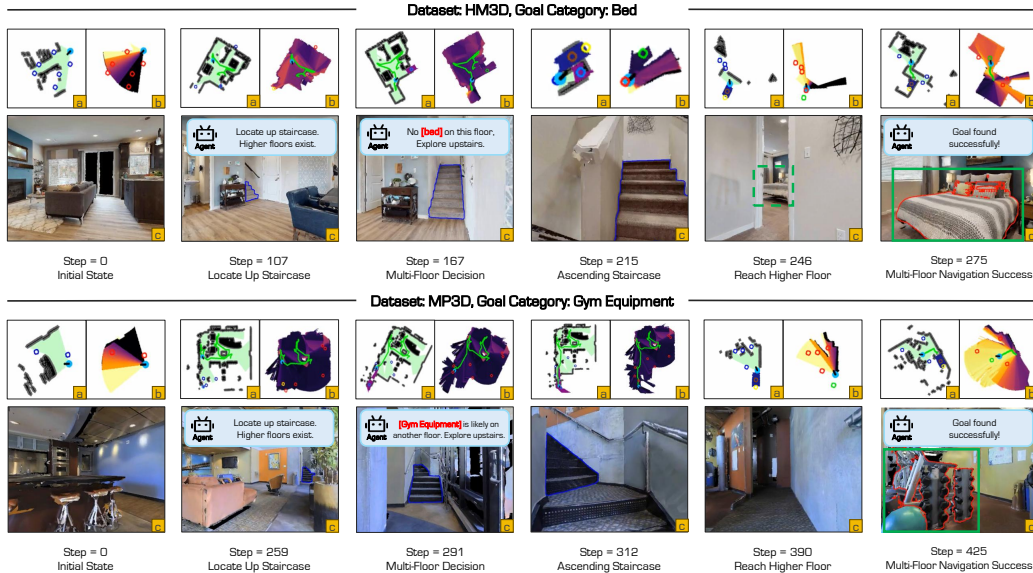


Figure 9: **Cases Analysis for Stair Ascending.** **Top row:** After traversing the current floor, the agent makes a multi-floor decision to navigate upstairs and successfully find the goal on a higher floor in the HM3D dataset. **Bottom row:** The agent actively infers that the target is on a higher floor and decides to ascend, successfully navigating to the goal on a higher floor in the MP3D dataset.

count exceeds τ_{floor} steps and the time since the last floor decision exceeds τ_{period} steps (triggering the LLM’s multi-floor decision), as shown in the example of the bottom row in Fig. 9.

During the transition, the agent treats the centroid of the stair as its initial waypoint and marks the entry point when its centroid enters the stair region. When stair pixels in the upper half image exceed a threshold ϵ_{up} , the agent executes a LOOK-UP action to prevent the pretrained PointNav model from mistaking the stair for an obstacle. After reaching the centroid of the stair, it navigates using dynamically updated waypoints (σ meters ahead) as described in Sec. 3. The exit point is marked when the centroid fully leaves the stair region. This process ensures smooth and accurate navigation through the stair region.

After ascending the stairs, the agent initializes the navigation stage on the new floor while establishing floor connectivity through bidirectional stair mapping using the BEV maps $\mathcal{M}_{obs}^{(2)}$ and $\mathcal{M}_{val}^{(2)}$. The higher floor’s down-stair parameters inherit the lower floor’s up-stair geometry with start/end points inverted while preserving the centroid. Navigation then continues with intra-floor rules, periodically invoking the LLM decision when unexplored floors remain in the exploration state.

C.5 Cases Analysis for Stair Descending

When the target is located on a lower floor, the agent must navigate downstairs. As shown in Fig. 10, the process for downstairs navigation is similar to that for ascending stairs, with the following adjustments:

Similarly, the agent operates under the assumption of a single floor, using BEV map lists $\mathcal{L}_{obs} = [\mathcal{M}_{obs}^{(1)}]$ and $\mathcal{L}_{val} = [\mathcal{M}_{val}^{(1)}]$. However, while it detects a down-stair region through depth inversion analysis, it transfer its current maps as $(\mathcal{M}_{obs}^{(2)}, \mathcal{M}_{val}^{(2)})$ and initializes maps for the lower floor $(\mathcal{M}_{obs}^{(1)}, \mathcal{M}_{val}^{(1)})$.

The agent initiates downstairs transition when either: (1) the current floor exploration completes while lower unexplored floors remain, as shown in the example of the top row in Fig. 10; or (2) the step count exceeds τ_{floor} steps and the time since the last floor decision exceeds τ_{period} steps (triggering the LLM’s multi-floor decision), as shown in the example of the bottom row in Fig. 10.

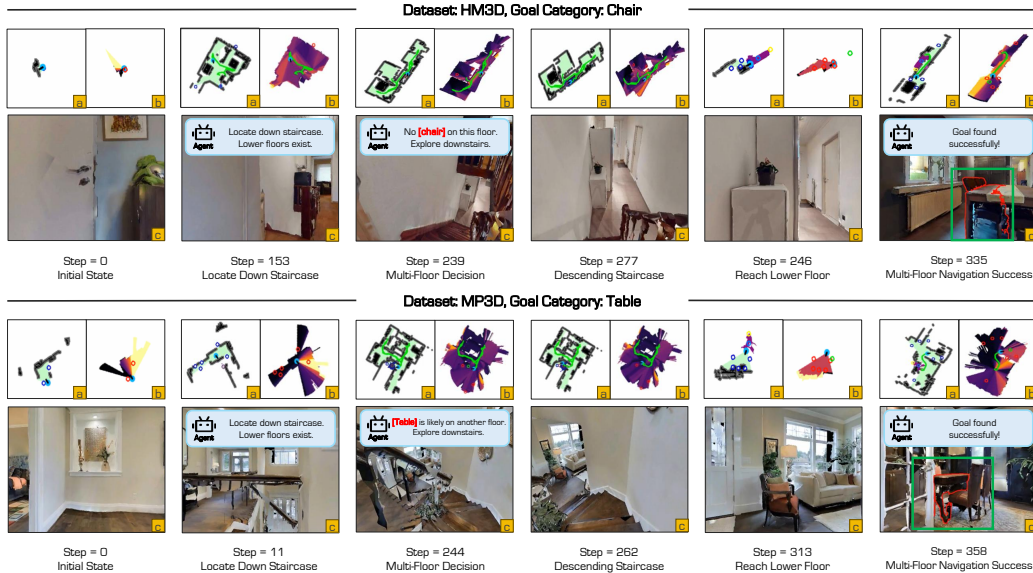


Figure 10: **Cases Analysis for Stair Descending.** **Top row:** After traversing the current floor, the agent makes a multi-floor decision to navigate downstairs and successfully find the goal on a lower floor in the HM3D dataset. **Bottom row:** The agent actively infers that the target is on a lower floor and decides to descend, successfully navigating to the goal on a lower floor in the MP3D dataset.

During the transition, the agent treats the centroid of the stair as its initial waypoint and marks the entry point when its centroid enters the stair region. When stair pixels in the lower half image are fewer than a threshold ϵ_{down} , the agent executes a LOOK-DOWN action to prevent losing the view of staircases. When stair pixels in the upper half image exceed a threshold ϵ_{up} , the agent executes a LOOK-UP action to prevent the pretrained PointNav model from mistaking the stair for an obstacle. After reaching the centroid of the stair, it navigates using dynamically updated waypoints (σ meters ahead) as described in Sec. 3. The exit point is marked when the centroid fully leaves the stair region. This process ensures smooth and accurate navigation through the stair region.

After descending the stairs, the agent initializes the navigation stage on the new floor while establishing floor connectivity through bidirectional stair mapping using the BEV maps $\mathcal{M}_{obs}^{(1)}$ and $\mathcal{M}_{val}^{(1)}$. The lower floor’s upstairs parameters inherit the higher floor’s down-stair geometry with start/end points inverted while preserving the centroid. Navigation then continues with intra-floor rules, periodically invoking the LLM decision when unexplored floors remain in the exploration state.

C.6 Cases Analysis for Stairwells

The agent may initialize its navigation within a stairwell, either positioned on a landing between stair flights (Fig. 11, top) or directly inside the stair section (Fig. 11, bottom). Due to limited initial contextual information of the scenario environment, we incorporate prior floor knowledge with the specific goal into the LLM. When the agent detects both ascending and descending staircases, this prior knowledge informs the LLM’s multi-floor decision-making process, enabling probabilistic estimation of the target’s vertical location (upstairs vs. downstairs). This optimization significantly improves navigation efficiency.

C.7 Cases Analysis for Floor Revisiting

As shown in Fig. 12, these cases demonstrate the effectiveness and robustness of our algorithm in multi-floor navigation.

The top row of examples is from the scene of the HM3D dataset. The agent initially leverages prior floor knowledge to make multi-floor decisions. After an unsuccessful search on the higher floor, the system actively reevaluates its strategy and successfully relocates the target might on the lower floor

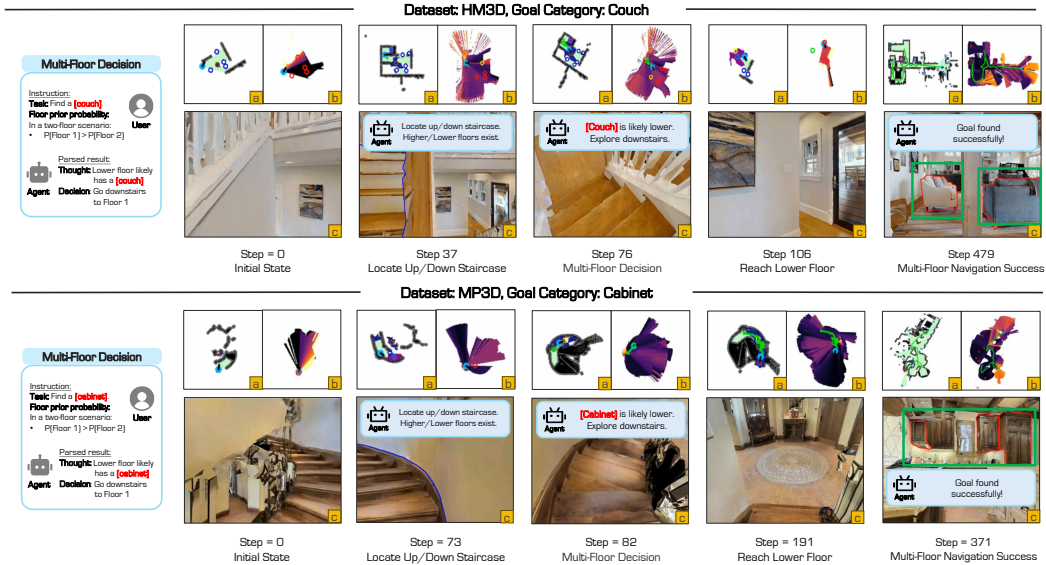


Figure 11: **Cases Analysis for Stairwells:** These examples illustrate the agent’s capability to make multi-floor decisions despite limited environmental context. **Top row:** Starting on a landing between stair flights in the HM3D dataset, the agent leverages prior floor knowledge to make a multi-floor decision, navigate downstairs, and successfully locate the goal on a lower floor. **Bottom row:** Beginning within the stair area in MP3D, the agent proactively infers that the goal is likely on a lower floor, leading to a multi-floor decision to navigate downwards and successfully reach the goal.

through a timely floor revisit. This adaptive behavior demonstrates the algorithm’s robustness in recovering from initial decision inaccuracies.

The bottom row presents a more complex case with dual staircases connecting the first and second floors from the MP3D dataset. The scene has two staircases between the 1st floor and the 2nd floor. Following partial exploration of the first floor, the agent prioritizes searching the second floor based on prior probability estimates. After searching for a while on the 2nd floor but not finding the target object, the agent needs to choose to go up to the 3rd floor or down to the 1st floor. Because the prior knowledge suggests that the probability of finding the target on the 1st floor is higher than that on the 3rd floor, the agent revisits the 1st floor from another staircase and successfully reaches the target, which validates both the effectiveness of our probability-driven approach and the algorithm’s capability to handle architectural complexities.

D Discussions & Limitations

While our method demonstrates effective multi-floor navigation capabilities, several limitations merit discussion. First, the accuracy of stair detection and floor perception remains imperfect, as evidenced shown in Tab. 8 by our evaluation on HM3D multi-floor episodes. The current system achieves 66.7% correct stair detection, but suffers from 20% false positives where non-stair structures are misclassified as stairs or stair directions are inverted, along with 13.3% missed detections where existing stairs go unrecognized. These errors primarily emerge from challenging visual conditions such as occluded stairwells, ambiguous depth signatures in corner cases, and visual similarities between stairs and other architectural features like ramps or platforms. Although our floor revisiting mechanism provides robustness against such detection failures, future improvements could explore multi-modal sensor fusion or temporal consistency checks to enhance reliability.

Table 8: Stair detection performance in a subset of the HM3D multi-floor scenes.

Metric	Value (%)
True Positive (Correct detection)	66.7
False Positive (Misclassification)	20.0
True Negative (Missed detection)	13.3

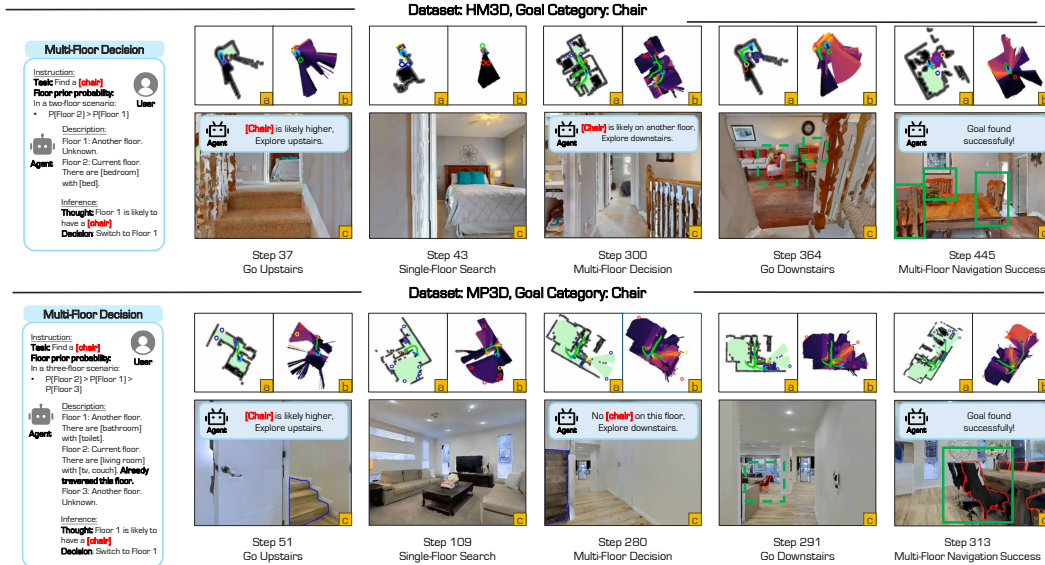


Figure 12: **Cases Analysis for Floor Revisiting:** These examples show the agent revisiting floors in complex multi-floor scenarios, illustrating the robustness of our algorithm. **Top row:** This example from the HM3D dataset, where the agent initially makes the wrong multi-floor decision but eventually successfully finds the target object through floor revisiting. **Bottom row:** In an example from the MP3D dataset featuring a scenario with multiple staircases connecting the first and second floors, the agent is still capable of revisiting the first floor and successfully reaching the target.

Second, the system’s dependence on prior knowledge about object distributions presents inherent constraints. While we employ both dataset-derived priors from training statistics and support user-defined custom priors - and have experimentally verified their utility through ablation studies - these priors are fundamentally limited by potential mismatches between training and testing environments. For example, the statistical regularities observed in residential settings may not perfectly transfer to office environments, and user-provided priors may reflect incomplete or biased assumptions. Our design mitigates these concerns through two key mechanisms: the system can override initial priors when accumulated evidence during an episode contradicts them, and the floor revisiting capability allows recovery from decisions based on inaccurate initial assumptions. The supplementary experiments demonstrate that while imperfect, these priors still provide positive guidance compared to purely reactive approaches, particularly in the early stages of exploration when contextual information remains scarce.

E Detailed Prompt Design

In this work, we design structured prompts to facilitate zero-shot multi-floor object navigation, enabling the model to identify target objects and select optimal floors without prior training on the specific environment. As illustrated in Tab. 9 and Tab. 10, these prompts include several key components, which are summarized as follows:

- **Task Specification:** The prompt begins by defining the task as selecting the optimal floor for navigating to a target object based on prior probabilistic data and environmental context. This specification is crucial for setting the objective and ensuring that the model’s actions align with the zero-shot navigation goal, where the model must generalize to unseen environments.
- **Expected Output Format:** The prompt explicitly specifies that the model’s response should be structured in JSON format. This ensures that the output is machine-readable and facilitates downstream processing and analysis. The structured format also enhances interpretability and consistency in the model’s responses, which is critical for zero-shot scenarios where reliability is paramount.
- **Example Input:** The prompt provides a detailed example input in JSON format, including the target object, prior probabilities associating floors and room types with the target object, and descriptions of each floor. This example serves as a reference for the model, illustrating the type of data it should expect and how to interpret it in the absence of prior training on the specific environment.
- **Example Response:** The prompt includes an example response in JSON format, containing the selected floor index and a justification for the selection. This demonstrates how the model should format its output and reason about the input data, ensuring transparency and verifiability in the decision-making process. For instance, the model might justify its choice by stating that a specific floor has the highest probability of containing the target object based on the provided data.
- **Template for Prompted Input:** A template is provided for the actual input, using placeholders such as `{{target_object_category}}`, `{{floor_prob_entries}}`, `{{prob_entries}}`, and `{{floor_entries}}`. This template ensures flexibility, allowing the prompt to be adapted to different environments and scenarios while maintaining a consistent structure. This is particularly important for zero-shot navigation, where the model must handle diverse and unseen environments.

These components are meticulously designed to guide the model in leveraging both probabilistic data and environmental context for zero-shot multi-floor object navigation. The structured format not only ensures clarity and consistency in the model responses but also facilitates effective communication and decision-making in unseen environments. By providing a comprehensive framework, the prompts enable the model to perform complex reasoning tasks with precision and reliability, which is critical for zero-shot navigation applications requiring high accuracy and interpretability.

Table 9: An example of the instruction for single-floor object navigation.

Task: Select the optimal area based on prior probabilistic data and environmental context.

Expected Answer Format: JSON

Example Input:

```
{
  "Goal": "toilet",
  "Prior Probabilities between Room Type and Goal Object": [
    "Bathroom": 90.0%,
    "Bedroom": 10.0%
  ],
  "Area Descriptions": [
    "Area 1": "a bathroom containing objects: shower, towel",
    "Area 2": "a bedroom containing objects: bed, nightstand",
    "Area 3": "a garage containing objects: car"
  ]
}
```

Example Response:

```
{
  "Index": "1",
  "Reason": "Shower and towel in Bathroom indicate toilet location,
            with high probability (90.0%)."
```

Prompted Input:

```
{
  "Goal": "{{target_object_category}}",
  "Prior Probabilities between Room Type and Goal Object": [
    {{prob_entries}}
  ],
  "Area Descriptions": [
    {{area_entries}}
  ]
}
```

Table 10: An example of the instruction for multi-floor object navigation.

Task: Select the optimal floor based on prior probabilistic data and environmental context.

Expected Answer Format: JSON

Example Input:

```
{
  "Goal": "bed",
  "Prior Probabilities between Floor and Goal Object": [
    "Floor 1": 10.0%,
    "Floor 2": 10.0%,
    "Floor 3": 80.0%
  ],
  "Prior Probabilities between Room Type and Goal Object": [
    "Bedroom": 80.0%,
    "Living room": 15.0%,
    "Bathroom": 5.0%
  ],
  "Floor Descriptions": [
    "Floor 1": "Current floor. There are room types: hall, living
              room, containing objects: tv, sofa",
    "Floor 2": "Other floor. There are room types: bathroom
              containing objects: shower, towel.
              You do not need to explore this floor again",
    "Floor 3": "Other floor. There are room types: unknown rooms
              containing objects: unknown objects"
  ]
}
```

Example Response:

```
{
  "Index": "3",
  "Reason": "The bedroom is most likely to be on the Floor 3,
            and the room types and object types on the Floor 1
            and Floor 2 are not directly related to the target
            object bed, especially it does not need to explore
            Floor 2 again."
}
```

Prompted Input:

```
{
  "Goal": "{{target_object_category}}",
  "Prior Probabilities between Floor and Goal Object": [
    {{floor_prob_entries}}
  ],
  "Prior Probabilities between Room Type and Goal Object": [
    {{prob_entries}}
  ],
  "Floor Descriptions": [
    {{floor_entries}}
  ]
}
```

References

- [1] Josh Achiam, Steven Adler, Sandhini Agarwal, Lama Ahmad, Ilge Akkaya, Florencia Leoni Aleman, Diogo Almeida, Janko Altenschmidt, Sam Altman, Shyamal Anadkat, et al. Gpt-4 technical report. *arXiv preprint arXiv:2303.08774*, 2023.
- [2] Ziad Al-Halah, Santhosh Kumar Ramakrishnan, and Kristen Grauman. Zero experience required: Plug & play modular transfer learning for semantic visual navigation. In *IEEE/CVF Conference on Computer Vision and Pattern Recognition*, pages 17031–17041, 2022.
- [3] Peter Anderson, Angel Chang, Devendra Singh Chaplot, Alexey Dosovitskiy, Saurabh Gupta, Vladlen Koltun, Jana Kosecka, Jitendra Malik, Roozbeh Mottaghi, Manolis Savva, et al. On evaluation of embodied navigation agents. *arXiv preprint arXiv:1807.06757*, 2018.
- [4] Peter Anderson, Qi Wu, Damien Teney, Jake Bruce, Mark Johnson, Niko Sünderhauf, Ian Reid, Stephen Gould, and Anton Van Den Hengel. Vision-and-language navigation: Interpreting visually-grounded navigation instructions in real environments. In *IEEE/CVF Conference on Computer Vision and Pattern Recognition*, pages 3674–3683, 2018.
- [5] Jinze Bai, Shuai Bai, Shusheng Yang, Shijie Wang, Sinan Tan, Peng Wang, Junyang Lin, Chang Zhou, and Jingren Zhou. Qwen-vl: A versatile vision-language model for understanding, localization. *arXiv preprint arXiv:2308.12966*, 2023.
- [6] Dhruv Batra, Aaron Gokaslan, Aniruddha Kembhavi, Oleksandr Maksymets, Roozbeh Mottaghi, Manolis Savva, Alexander Toshev, and Erik Wijmans. Objectnav revisited: On evaluation of embodied agents navigating to objects. *arXiv preprint arXiv:2006.13171*, 2020.
- [7] Cesar Cadena, Luca Carlone, Henry Carrillo, Yasir Latif, Davide Scaramuzza, José Neira, Ian Reid, and John J Leonard. Past, present, and future of simultaneous localization and mapping: Toward the robust-perception age. *IEEE Transactions on robotics*, 32(6):1309–1332, 2016.
- [8] Wenzhe Cai, Siyuan Huang, Guangran Cheng, Yuxing Long, Peng Gao, Changyin Sun, and Hao Dong. Bridging zero-shot object navigation and foundation models through pixel-guided navigation skill. In *IEEE International Conference on Robotics and Automation*, pages 5228–5234, 2024.
- [9] Angel Chang, Angela Dai, Thomas Funkhouser, Maciej Halber, Matthias Niessner, Manolis Savva, Shuran Song, Andy Zeng, and Yinda Zhang. Matterport3d: Learning from rgb-d data in indoor environments. *arXiv preprint arXiv:1709.06158*, 2017.
- [10] Devendra Singh Chaplot, Dhiraj Prakashchand Gandhi, Abhinav Gupta, and Russ R Salakhutdinov. Object goal navigation using goal-oriented semantic exploration. *Advances in Neural Information Processing Systems*, 33:4247–4258, 2020.
- [11] Hongyi Chen, Ruinian Xu, Shuo Cheng, Patricio A Vela, and Danfei Xu. Zero-shot object searching using large-scale object relationship prior. *arXiv preprint arXiv:2303.06228*, 2023.
- [12] Junting Chen, Guohao Li, Suryansh Kumar, Bernard Ghanem, and Fisher Yu. How to not train your dragon: Training-free embodied object goal navigation with semantic frontiers. *arXiv preprint arXiv:2305.16925*, 2023.
- [13] Shizhe Chen, Thomas Chabal, Ivan Laptev, and Cordelia Schmid. Object goal navigation with recursive implicit maps. In *2023 IEEE/RSJ International Conference on Intelligent Robots and Systems (IROS)*, pages 7089–7096. IEEE, 2023.
- [14] Jacob Devlin, Ming-Wei Chang, Kenton Lee, and Kristina Toutanova. Bert: Pre-training of deep bidirectional transformers for language understanding. In *Conference of the North American Chapter of the Association for Computational Linguistics*, pages 4171–4186, 2019.
- [15] Zhicheng Feng, Xieyuanli Chen, Chenghao Shi, Lun Luo, Zhichao Chen, Yun-Hui Liu, and Huimin Lu. Image-goal navigation using refined feature guidance and scene graph enhancement. *arXiv preprint arXiv:2503.10986*, 2025.
- [16] Samir Yitzhak Gadre, Mitchell Wortsman, Gabriel Ilharco, Ludwig Schmidt, and Shuran Song. Cows on pasture: Baselines and benchmarks for language-driven zero-shot object navigation. In *IEEE/CVF Conference on Computer Vision and Pattern Recognition*, pages 23171–23181, 2023.
- [17] Zeying Gong, Tianshuai Hu, Ronghe Qiu, and Junwei Liang. From cognition to precognition: A future-aware framework for social navigation. *arXiv preprint arXiv:2409.13244*, 2024.
- [18] Jesse Haviland, Niko Sünderhauf, and Peter Corke. A holistic approach to reactive mobile manipulation. *IEEE Robotics and Automation Letters*, 7(2):3122–3129, 2022.
- [19] Tianshuai Hu, Jianhao Jiao, Yucheng Xu, Hongji Liu, Sheng Wang, and Ming Liu. Dhp-mapping: A dense panoptic mapping system with hierarchical world representation and label optimization techniques. In *2024 IEEE/RSJ International Conference on Intelligent Robots and Systems (IROS)*, pages 1101–1107. IEEE, 2024.

- [20] Jindong Jiang, Lunan Zheng, Fei Luo, and Zhijun Zhang. Rednet: Residual encoder-decoder network for indoor rgb-d semantic segmentation. *arXiv preprint arXiv:1806.01054*, 2018.
- [21] KJ Joseph, Salman Khan, Fahad Shahbaz Khan, and Vineeth N Balasubramanian. Towards open world object detection. In *IEEE/CVF Conference on Computer Vision and Pattern Recognition*, pages 5830–5840, 2021.
- [22] Mukul Khanna, Ram Ramrakhya, Gunjan Chhablani, Sriram Yenamandra, Theophile Gervet, Matthew Chang, Zsolt Kira, Devendra Singh Chaplot, Dhruv Batra, and Roozbeh Mottaghi. Goat-bench: A benchmark for multi-modal lifelong navigation. In *IEEE/CVF Conference on Computer Vision and Pattern Recognition*, pages 16373–16383, 2024.
- [23] Junnan Li, Dongxu Li, Silvio Savarese, and Steven Hoi. Blip-2: Bootstrapping language-image pre-training with frozen image encoders and large language models. In *International Conference on Machine Learning*, pages 19730–19742. PMLR, 2023.
- [24] Junnan Li, Dongxu Li, Caiming Xiong, and Steven Hoi. Blip: Bootstrapping language-image pre-training for unified vision-language understanding and generation. In *International Conference on Machine Learning*, pages 12888–12900. PMLR, 2022.
- [25] Rong Li, Shijie Li, Lingdong Kong, Xulei Yang, and Junwei Liang. Seeground: See and ground for zero-shot open-vocabulary 3d visual grounding. *arXiv preprint arXiv:2412.04383*, 2024.
- [26] Rong Li, Shijie Li, Lingdong Kong, Xulei Yang, and Junwei Liang. Zero-shot 3d visual grounding from vision-language models. *arXiv preprint arXiv:2505.22429*, 2025.
- [27] Tsung-Yi Lin, Michael Maire, Serge Belongie, James Hays, Pietro Perona, Deva Ramanan, Piotr Dollár, and C Lawrence Zitnick. Microsoft coco: Common objects in context. In *Computer vision—ECCV 2014: 13th European conference, zurich, Switzerland, September 6–12, 2014, proceedings, part v 13*, pages 740–755. Springer, 2014.
- [28] Haotian Liu, Chunyuan Li, Qingyang Wu, and Yong Jae Lee. Visual instruction tuning. *Advances in neural information processing systems*, 36:34892–34916, 2023.
- [29] Shilong Liu, Zhaoyang Zeng, Tianhe Ren, Feng Li, Hao Zhang, Jie Yang, Qing Jiang, Chunyuan Li, Jianwei Yang, Hang Su, et al. Grounding dino: Marrying dino with grounded pre-training for open-set object detection. In *European Conference on Computer Vision*, pages 38–55. Springer, 2024.
- [30] Yinhan Liu, Myle Ott, Naman Goyal, Jingfei Du, Mandar Joshi, Danqi Chen, Omer Levy, Mike Lewis, Luke Zettlemoyer, and Veselin Stoyanov. Roberta: A robustly optimized bert pretraining approach. *arXiv preprint arXiv:1907.11692*, 2019.
- [31] Yuxing Long, Wenzhe Cai, Hongcheng Wang, Guanqi Zhan, and Hao Dong. Instructnav: Zero-shot system for generic instruction navigation in unexplored environment. In *Conference on Robot Learning*, 2024.
- [32] Arjun Majumdar, Gunjan Aggarwal, Bhavika Devnani, Judy Hoffman, and Dhruv Batra. Zson: Zero-shot object-goal navigation using multimodal goal embeddings. *Advances in Neural Information Processing Systems*, 35:32340–32352, 2022.
- [33] Raul Mur-Artal and Juan D Tardós. Orb-slam2: An open-source slam system for monocular, stereo, and rgb-d cameras. *IEEE transactions on robotics*, 33(5):1255–1262, 2017.
- [34] Long Ouyang, Jeffrey Wu, Xu Jiang, Diogo Almeida, Carroll Wainwright, Pamela Mishkin, Chong Zhang, Sandhini Agarwal, Katarina Slama, Alex Ray, et al. Training language models to follow instructions with human feedback. *Advances in Neural Information Processing Systems*, 35:27730–27744, 2022.
- [35] Yansong Peng, Hebei Li, Peixi Wu, Yueyi Zhang, Xiaoyan Sun, and Feng Wu. D-fine: redefine regression task in detr as fine-grained distribution refinement. *arXiv preprint arXiv:2410.13842*, 2024.
- [36] Xavier Puig, Eric Undersander, Andrew Szot, Mikael Dallahire Cote, Tsung-Yen Yang, Ruslan Partsey, Ruta Desai, Alexander William Clegg, Michal Hlavac, So Yeon Min, et al. Habitat 3.0: A co-habitat for humans, avatars and robots. *arXiv preprint arXiv:2310.13724*, 2023.
- [37] Alec Radford, Jong Wook Kim, Chris Hallacy, Aditya Ramesh, Gabriel Goh, Sandhini Agarwal, Girish Sastry, Amanda Askell, Pamela Mishkin, Jack Clark, et al. Learning transferable visual models from natural language supervision. In *International Conference on Machine Learning*, pages 8748–8763. PmLR, 2021.
- [38] Santhosh K Ramakrishnan, Aaron Gokaslan, Erik Wijmans, Oleksandr Maksymets, Alex Clegg, John Turner, Eric Undersander, Wojciech Galuba, Andrew Westbury, Angel X Chang, et al. Habitat-matterport 3d dataset (hm3d): 1000 large-scale 3d environments for embodied ai. *arXiv preprint arXiv:2109.08238*, 2021.
- [39] Santhosh Kumar Ramakrishnan, Devendra Singh Chaplot, Ziad Al-Halah, Jitendra Malik, and Kristen Grauman. Poni: Potential functions for objectgoal navigation with interaction-free learning. In *IEEE/CVF Conference on Computer Vision and Pattern Recognition*, pages 18890–18900, 2022.

- [40] Ram Ramrakhya, Dhruv Batra, Erik Wijmans, and Abhishek Das. Pirlnav: Pretraining with imitation and rl finetuning for objectnav. In *IEEE/CVF Conference on Computer Vision and Pattern Recognition*, pages 17896–17906, 2023.
- [41] Ram Ramrakhya, Eric Undersander, Dhruv Batra, and Abhishek Das. Habitat-web: Learning embodied object-search strategies from human demonstrations at scale. In *IEEE/CVF Conference on Computer Vision and Pattern Recognition*, pages 5173–5183, 2022.
- [42] Manolis Savva, Abhishek Kadian, Oleksandr Maksymets, Yili Zhao, Erik Wijmans, Bhavana Jain, Julian Straub, Jia Liu, Vladlen Koltun, Jitendra Malik, et al. Habitat: A platform for embodied ai research. In *IEEE/CVF International Conference on Computer Vision*, pages 9339–9347, 2019.
- [43] Jingwen Sun, Jing Wu, Ze Ji, and Yu-Kun Lai. A survey of object goal navigation. *IEEE Transactions on Automation Science and Engineering*, 2024.
- [44] Xinyu Sun, Lizhao Liu, Hongyan Zhi, Ronghe Qiu, and Junwei Liang. Prioritized semantic learning for zero-shot instance navigation. In *European Conference on Computer Vision*, pages 161–178. Springer, 2024.
- [45] Hugo Touvron, Thibaut Lavril, Gautier Izacard, Xavier Martinet, Marie-Anne Lachaux, Timothée Lacroix, Baptiste Rozière, Naman Goyal, Eric Hambro, Faisal Azhar, et al. Llama: Open and efficient foundation language models. *arXiv preprint arXiv:2302.13971*, 2023.
- [46] Chien-Yao Wang, Alexey Bochkovskiy, and Hong-Yuan Mark Liao. Yolov7: Trainable bag-of-freebies sets new state-of-the-art for real-time object detectors. In *Proceedings of the IEEE/CVF conference on computer vision and pattern recognition*, pages 7464–7475, 2023.
- [47] Dewei Wang, Jiaming Chen, and Jiyu Cheng. A survey of object goal navigation: Datasets, metrics and methods. In *IEEE International Conference on Mechatronics and Automation*, pages 2171–2176, 2023.
- [48] Zhou Wang, Alan C Bovik, Hamid R Sheikh, and Eero P Simoncelli. Image quality assessment: from error visibility to structural similarity. *IEEE transactions on image processing*, 13(4):600–612, 2004.
- [49] Justin Wasserman, Girish Chowdhary, Abhinav Gupta, and Unnat Jain. Exploitation-guided exploration for semantic embodied navigation. In *IEEE International Conference on Robotics and Automation*, pages 2901–2908, 2024.
- [50] Luca Weihs, Unnat Jain, Iou-Jen Liu, Jordi Salvador, Svetlana Lazebnik, Aniruddha Kembhavi, and Alex Schwing. Bridging the imitation gap by adaptive insubordination. *Advances in Neural Information Processing Systems*, 34:19134–19146, 2021.
- [51] Pengying Wu, Yao Mu, Bingxian Wu, Yi Hou, Ji Ma, Shanghang Zhang, and Chang Liu. Voronav: voronoi-based zero-shot object navigation with large language model. In *International Conference on Machine Learning*, pages 53737–53775. PMLR, 2024.
- [52] Karmesh Yadav, Jacob Krantz, Ram Ramrakhya, Santhosh Kumar Ramakrishnan, Jimmy Yang, Austin Wang, John Turner, Aaron Gokaslan, Vincent-Pierre Berges, Roozbeh Mootaghi, Oleksandr Maksymets, Angel X. Chang, Manolis Savva, Alexander Clegg, Devendra Singh Chaplot, and Dhruv Batra. Habitat Challenge 2023. <https://aihabitat.org/challenge/2023/>, 2023.
- [53] Karmesh Yadav, Arjun Majumdar, Ram Ramrakhya, Naoki Yokoyama, Alexei Baevski, Zsolt Kira, Oleksandr Maksymets, and Dhruv Batra. Ovrl-v2: A simple state-of-art baseline for imagenav and objectnav. *arXiv preprint arXiv:2303.07798*, 2023.
- [54] Karmesh Yadav, Santhosh Kumar Ramakrishnan, John Turner, Aaron Gokaslan, Oleksandr Maksymets, Rishabh Jain, Ram Ramrakhya, Angel X. Chang, Alexander Clegg, Manolis Savva, Eric Undersander, Devendra Singh Chaplot, and Dhruv Batra. Habitat Challenge 2022. <https://aihabitat.org/challenge/2022/>, 2022.
- [55] Karmesh Yadav, Ram Ramrakhya, Arjun Majumdar, Vincent-Pierre Berges, Sachit Kuhar, Dhruv Batra, Alexei Baevski, and Oleksandr Maksymets. Offline visual representation learning for embodied navigation. In *International Conference on Learning Representations Workshop*, 2023.
- [56] An Yang, Baosong Yang, Beichen Zhang, Binyuan Hui, Bo Zheng, Bowen Yu, Chengyuan Li, Dayiheng Liu, Fei Huang, Haoran Wei, et al. Qwen2.5 technical report. *arXiv preprint arXiv:2412.15115*, 2024.
- [57] Joel Ye, Dhruv Batra, Abhishek Das, and Erik Wijmans. Auxiliary tasks and exploration enable objectgoal navigation. In *IEEE/CVF International Conference on Computer Vision*, pages 16117–16126, 2021.
- [58] Hang Yin, Xiuwei Xu, Zhenyu Wu, Jie Zhou, and Jiwen Lu. Sg-nav: Online 3d scene graph prompting for llm-based zero-shot object navigation. *Advances in Neural Information Processing Systems*, 37:5285–5307, 2024.
- [59] Hang Yin, Xiuwei Xu, Lingqing Zhao, Ziwei Wang, Jie Zhou, and Jiwen Lu. Unigoal: Towards universal zero-shot goal-oriented navigation. *arXiv preprint arXiv:2503.10630*, 2025.

- [60] Naoki Yokoyama, Sehoon Ha, Dhruv Batra, Jiuguang Wang, and Bernadette Bucher. Vlfm: Vision-language frontier maps for zero-shot semantic navigation. In *IEEE International Conference on Robotics and Automation*, pages 42–48, 2024.
- [61] Bangguo Yu, Hamidreza Kasaei, and Ming Cao. L3mvm: Leveraging large language models for visual target navigation. In *IEEE/RSJ International Conference on Intelligent Robots and Systems*, pages 3554–3560, 2023.
- [62] Shuaihang Yuan, Hao Huang, Yu Hao, Congcong Wen, Anthony Tzes, and Yi Fang. Gamap: Zero-shot object goal navigation with multi-scale geometric-affordance guidance. In *Advances in Neural Information Processing Systems*, volume 37, 2024.
- [63] Chaoning Zhang, Dongshen Han, Yu Qiao, Jung Uk Kim, Sung-Ho Bae, Seungkyu Lee, and Choong Seon Hong. Faster segment anything: Towards lightweight sam for mobile applications. *arXiv preprint arXiv:2306.14289*, 2023.
- [64] Lingfeng Zhang, Hao Wang, Erjia Xiao, Xinyao Zhang, Qiang Zhang, Zixuan Jiang, and Renjing Xu. Multi-floor zero-shot object navigation policy. *arXiv preprint arXiv:2409.10906*, 2024.
- [65] Lingfeng Zhang, Qiang Zhang, Hao Wang, Erjia Xiao, Zixuan Jiang, Honglei Chen, and Renjing Xu. Trihelper: Zero-shot object navigation with dynamic assistance. In *IEEE/RSJ International Conference on Intelligent Robots and Systems*, pages 10035–10042, 2024.
- [66] Renrui Zhang, Jiaming Han, Chris Liu, Peng Gao, Aojun Zhou, Xiangfei Hu, Shilin Yan, Pan Lu, Hongsheng Li, and Yu Qiao. Llama-adapter: Efficient fine-tuning of language models with zero-init attention. *arXiv preprint arXiv:2303.16199*, 2023.
- [67] Sixian Zhang, Weijie Li, Xinhang Song, Yubing Bai, and Shuqiang Jiang. Generative meta-adversarial network for unseen object navigation. In *European Conference on Computer Vision*, pages 301–320. Springer, 2022.
- [68] Qianfan Zhao, Lu Zhang, Bin He, Hong Qiao, and Zhiyong Liu. Zero-shot object goal visual navigation. In *IEEE International Conference on Robotics and Automation*, pages 2025–2031, 2023.
- [69] Kaiwen Zhou, Kaizhi Zheng, Connor Pryor, Yilin Shen, Hongxia Jin, Lise Getoor, and Xin Eric Wang. Esc: Exploration with soft commonsense constraints for zero-shot object navigation. In *International Conference on Machine Learning*, pages 42829–42842. PMLR, 2023.